Effects of weak anchoring on the equivalent anchoring energy in a nematic cell with large amplitude of the grooves

Effects of weak anchoring on the equivalent anchoring energy in a nematic cell with large amplitude of the grooves

G. Barbero, A. S. Gliozzi, and M. Scalerandi[a)]
Dipartimento di Fisica del Politecnico, Corso Duca degli Abruzzi, 24-10129 Torino, Italy

(Received 20 June 2008; accepted 9 September 2008; published online 6 November 2008)

Nanostructured corrugated surfaces in liquid crystal cells have a strong influence on the alignment of liquid crystal molecules. An equivalent energy can be attributed to the system due to deformations resulting from the equilibrium between bulk elastic forces and surface forces due to the anchoring of the molecules to the layer. First, we derive the equilibrium equations on the surface and in the bulk for a cell with a corrugated surface with large amplitude A of the grooves and weak anchoring. We also analyze numerically the solution and show that the equivalent anchoring energy presents a nontrivial dependence on A and falls to zero for infinite amplitude grooves. © *2008 American Institute of Physics*. [DOI: 10.1063/1.3005982]

I. INTRODUCTION

Inhomogeneous or nanotextured surfaces in liquid crystal cells have a significant effect on the alignment of liquid crystal molecules.[1–6] A competition arises between elastic restoring forces and the contribution due to the surface topography on the molecular orientation of the liquid-crystalline phases.[7–10] In the past years, this problem has become of practical importance, since photoalignment techniques have been developed as a convenient method to homogeneously align liquid crystals.[11–13] The drawback is that rubbing of the substrate causes both elastic energy anisotropy, due to the morphology of the surface,[14,15] and anisotropic interaction between the liquid crystal molecules and the alignment layer surface.[16,17] It is therefore important to correctly estimate the total elastic energy in the sample and the equivalent anchoring energy strength.[18]

From the theoretical point of view, the first studies on the contribution of elastic origin to the surface energy of a nematic liquid crystal in the presence of a nonflat surface were conducted by Berreman.[19] In his analysis, he assumed that, in a first approximation, the surface can be described by a sinusoidal structure of wave vector $q=2\pi/\lambda$ and amplitude A, where λ is the spatial periodicity of the surface. This approximation is reasonable for common applications. On the contrary, the further approximations, necessary to obtain an exact solution, are often too strong.[17] Among them the small amplitude limit ($qA \ll 1$),[20] the isotropy of the elastic constants K_{ij} of the nematic molecules ($K=K_{11}=K_{22}=K_{33}$), and the strong anchoring hypotheses, i.e., the surface is such to fix the orientation of the nematic molecules parallel to the substrate.

Further developments have been proposed in the past years, but always in the limit $qA \ll 1$. Faetti[21] investigated how a finite polar anchoring and the reduced (or increased) surface order may affect the azimuthal anchoring, while Fournier and Galatola,[22] by means of a coarse-grained technique, derived an effective anchoring energy of a nematic liquid crystal in contact with a macroscopically corrugated surface including the anisotropy of the elastic constants. Finally, Fukuda *et al.*[23] showed that, differently from the assumption made in the original approach of Berreman,[19] the azimuthal distortion of the director cannot be considered as negligibly small.

As we have shown in Ref. 18, a meaningful solution cannot be obtained at the leading order in A: neglecting higher order terms leads to an overestimation of the exact equivalent anchoring energy. At the same time, the solution for large amplitude of the grooves can be obtained numerically, but a few nontrivial issues have to be considered to obtain a convergent numerical solution, as will be discussed here. In this contribution, we will also discuss the influence of the anchoring strength (at the rubbed surface) on the distribution of elastic energy density and on the equivalent anchoring energy strength. In our approach, the influence of the variations in the azimuthal angle is neglected, while the correct boundary conditions are derived using a variational analysis.

II. THEORY

A. Variational analysis

Let us consider a nematic liquid crystal limited by a grooved profile,

$$z_0(x) = A[1 + \cos(qx)]. \tag{1}$$

The direction of the grooves is assumed to be parallel to the y-axis of a Cartesian reference frame and we assume the system as two dimensional, when the (x,z)-plane contains the nematic director $\mathbf{n}(x,z)=\mathbf{u_x}\cos\theta(x,z)+\mathbf{u_z}\sin\theta(x,z)$, where θ is the tilt angle (see Fig. 1) and $\mathbf{u_x}$ and $\mathbf{u_z}$ are the unit vectors along the x- and z-axes, respectively. We assume the cell to be infinite in the x- and z-directions. The nematic deformation is periodic with spatial period λ. We limit our investigation to $0<x<\lambda$. Deformations are expected to decay rapidly when moving away from the surface. As we will show $0<z<2A+2\lambda$ is sufficient to approximate correctly an infinite medium. Let us consider the region $\mathcal{R}$, limited by the

a)Electronic mail: marco.scalerandi@infm.polito.it.

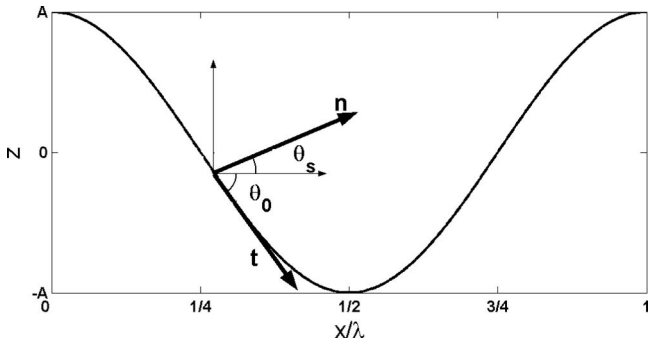

FIG. 1. Schematic representation of the surface, of the nematic (**n**), and tangent to the surface (**t**) directors.

profile (1) and by the two straight lines $x=0$ and $x=\lambda$. The border of $\mathcal{R}$ is indicated in the following by $\partial\mathcal{R}$.

The finite anchoring energy per unit area which accounts for the interaction of the nematic liquid crystal with the substrate is defined as

$$g = -\tfrac{1}{2}w_e(\mathbf{n}\cdot\mathbf{t})^2 = -\tfrac{1}{2}w_e\cos^2[\theta_s-\theta_0], \tag{2}$$

where w_e is the anchoring energy strength and **n** and **t** are the nematic director at the surface and the geometrical tangent to the profile, respectively. $\theta_s=\theta[x,z_0(x)]$ is the tilt angle on the boundary. We have also introduced on the boundary the angle

$$\theta_0(x) = \arctan[-qA\,\sin\,(qx)], \tag{3}$$

which corresponds to the tilt angle forced on the boundary in the case of strong anchoring hypotheses (orientation parallel to the surface).

As a consequence of the finite anchoring energy g, the director **n** is no longer parallel to **t** and a distribution $\theta(x,z)$ is originated inside the sample. The bulk elastic energy density f, in the one constant approximation,[20] is

$$f(x,z) = \frac{1}{2}K(\theta_{,x}^2+\theta_{,z}^2), \tag{4}$$

where $\theta_{,x}=\partial\theta/\partial x$ and $\theta_{,z}=\partial\theta/\partial z$. The total energy of the sample, per period and for unit length along the y-direction, is given by

$$F[\theta(x,z)] = \int\int_{\mathcal{R}} f(\theta,\nabla\theta)dxdz + \int_\gamma g(\theta)d\ell, \tag{5}$$

where γ is the line limiting $\mathcal{R}$ from below, and $d\ell=\sqrt{1+(dz_0/dx)^2}dx$.

The actual nematic orientation is the one minimizing F. We indicate by $\theta(x,z)$ the tilt angle minimizing F and by $\vartheta(x,z)=\theta(x,z)+\delta\vartheta(x,z)$ a function close to $\theta(x,z)$, in the variational sense. Since the problem presents a periodicity along the x-axis, with a spatial period λ, we look for a solution of the problem under consideration of the form $\vartheta(x,z)=\vartheta(x+\lambda,z)$. It follows also $\theta(x,z)=\theta(x+\lambda,z)$ and consequently, the arbitrary variations are such that $\delta\vartheta(x,z)=\delta\vartheta(x+\lambda,z)$. The first variation of $F[\vartheta(x,z)]$ given by Eq. (5) is

$$\delta F = \int\int_{\mathcal{R}}\left(\frac{\partial f}{\partial\vartheta}-\nabla\frac{\partial f}{\partial\nabla\vartheta}\right)_{\vartheta=\theta}\delta\vartheta dxdz + \int_{\partial R}\left(\mathbf{u}\cdot\frac{\partial f}{\partial\nabla\vartheta}\right)_{\vartheta=\theta}\delta\vartheta d\ell + \int_\gamma\left(\frac{dg}{d\vartheta_s}\right)_{\vartheta=\theta}\delta\vartheta_s d\ell, \tag{6}$$

where **u** is the geometrical normal to $\partial\mathcal{R}$, directed outward. Using Eq. (4), Eq. (6) can be rewritten as

$$\delta F = \int\int_{\mathcal{R}} -K\nabla^2\theta\delta\vartheta dxdz + \int_{\partial\mathcal{R}} K(\mathbf{u}\cdot\nabla\theta)\delta\vartheta d\ell + \int_\gamma\left(\frac{dg}{d\vartheta}\right)_{\vartheta=\theta}\delta\vartheta d\ell. \tag{7}$$

A simple calculation gives

$$\int_{\partial\mathcal{R}}(\mathbf{u}\cdot\nabla\theta)\delta\vartheta d\ell = \int_0^\infty\{\theta_{,x}(\lambda,z)\delta\vartheta(\lambda,z)-\theta_{,x}(0,z)\delta\vartheta(0,z)\}dz + \lim_{h\to\infty}\int_0^\lambda\theta_{,z}(x,h)\delta\vartheta(x,h)dx + \int_\gamma(\mathbf{u}\cdot\nabla\theta)\delta\vartheta d\ell. \tag{8}$$

From the discussion reported above on the periodicity along the x-axis of the solution we are looking for, it follows that

$$\theta_{,x}(\lambda,z)\delta\vartheta(\lambda,z)-\theta_{,x}(0,z)\delta\vartheta(0,z)=0. \tag{9}$$

Consequently, δF given by Eq. (6) can be rewritten as

$$\delta F = \int\int_{\mathcal{R}} -K\nabla^2\theta\delta\vartheta dxdz + \lim_{h\to\infty}\int_0^\lambda K\theta_{,z}(x,h)\delta\vartheta(x,h)dx + \int_\gamma\left\{K\mathbf{u}\cdot\nabla\theta+\left(\frac{dg}{d\vartheta}\right)_{\vartheta=\theta}\right\}\delta\vartheta[x,z_0(x)]d\ell. \tag{10}$$

By imposing $\delta F=0$ for all $\delta\vartheta$ of the class $\mathcal{C}_1$, i.e., continuous with its first order partial derivatives, we obtain that θ is the solution of the differential equation $\nabla^2\theta=0$ and satisfies the boundary conditions $\lim_{h\to\infty}\theta_{,z}(x,h)=0$ and $K(\mathbf{u}\cdot\nabla\theta)+(dg/d\vartheta)_{\vartheta=\theta}=0$ on the line γ.

Since $\mathbf{t}=\mathbf{u_x}\cos\theta_0+\mathbf{u_z}\sin\theta_0$, and on γ the geometrical normal (outward directed) as $\mathbf{u}=\mathbf{u_x}\sin\theta_0-\mathbf{u_z}\cos\theta_0$, where $\tan\theta_0(x)=dz_0(x)/dx$, the bulk equilibrium equation becomes

$$\theta_{,xx}+\theta_{,zz}=0, \tag{11}$$

which has to be solved with the boundary conditions

$$\lim_{z\to\infty}\theta_{,z}(x,z)=0, \tag{12}$$

and, by taking into account Eq. (2),

$$K\{\sin\,\theta_0\theta_{,x}-\cos\,\theta_0\theta_{,z}\}+(w_e/2)\sin[2(\theta-\theta_0)]=0, \tag{13}$$

on the line γ.

Equation (11) states that, in the configuration of equilibrium, the bulk density of mechanical torque vanishes,

whereas the boundary condition (13) implies that the elastic torque transmitted by the bulk to the surface is balanced by the surface torque due to the anisotropic interaction between the substrate and the nematic liquid crystal molecules. Finally, Eq. (12) defines the transversality condition for the functional Eq. (4), and physically means that the mechanical torque has to vanish at the infinity, where the system is not distorted.[24] Usually, deviations in the orientation of the nematic molecules vanish within a distance of a few wavelengths from the surface. Finally, the total energy of the sample, per period and for unit length along the y-direction, can be rewritten as

$$F[\theta(x,z)] = \int\int_{\mathcal{R}} \tfrac{1}{2}K(\theta_{,x}^2 + \theta_{,z}^2)dxdz + \int_{\gamma} -\tfrac{1}{2}w_e \cos^2[\theta_s - \theta_0]d\ell, \tag{14}$$

B. Definition of the equivalent anchoring energy

The system described in the previous Subsection is characterized by molecules with a nematic director perpendicular to the grooves. The total energy F contains two contributions: one is the bulk elastic energy and the second is the surface energy: Eq. (14).

A (trivial) equilibrium condition is that characterized by molecules on the surface aligned parallel to the grooves. In this case, $\theta_s=\theta=0$ everywhere. Since $\theta_0=0$ also, the total energy is $F_0=\int -(w_e/2)\,d\ell$. In fact, the elastic energy is zero.

Here, we introduce an equivalent anchoring energy w, defined as

$$w = 2\frac{F-F_0}{\lambda} = \frac{2}{\lambda}\left[\int\int_{\mathcal{R}} \frac{1}{2}K(\theta_{,x}^2 + \theta_{,z}^2)dxdz - \int_{\gamma}\frac{1}{2}w_e \sin^2[\theta_s - \theta_0]d\ell\right], \tag{15}$$

where we have used Eq. (14). In the equivalent anchoring energy w, we can distinguish two contributions, namely, the elastic bulk contribution G_B and the surface contribution G_S,

$$G_B = \int\int_{\mathcal{R}} \tfrac{1}{2}K(\theta_{,x}^2 + \theta_{,z}^2)dxdz$$

$$G_S = -\int_{\gamma} \tfrac{1}{2}w_e \sin^2[\theta_s - \theta_0]d\ell \tag{16}$$

C. Limit for small amplitude of the grooves

In the small amplitude limit ($qA \ll 1$), Eq. (11) with the boundary condition (13) can be solved analytically, with some approximations. In particular, in the strong anchoring case, corresponding to $w_e \to \infty$, the boundary conditions on γ are reduced to $\theta_s[x, z_0(x)] = \theta_0(x)$. Furthermore, we can also approximate $\theta_0(x)$ [given by Eq. (3)] as $\theta_0(x) \sim -qA \sin(qx)$. In this case, the analytical solution derived by Berreman[19] gives a tilt angle field

$$\theta(x,z) = -qA \sin(qx)\exp(-qz). \tag{17}$$

It follows that the bulk elastic energy density f is

$$f(x,z) = \tfrac{1}{2}K(\theta_{,x}^2 + \theta_{,z}^2) = \tfrac{1}{2}K(q^2A)^2 \exp(-2qz). \tag{18}$$

The total elastic energy per unit length along the y-axis per period is then

$$G_B = \int_0^{\lambda}\int_0^{\infty} f dxdz = \tfrac{1}{4}K\lambda(qA)^2 q. \tag{19}$$

Consequently the elastic energy per unit surface is $2G_B/\lambda$ and the equivalent anchoring energy is $w_B=(K/2)q(qA)^2$.

A similar solution can be given also for the weak anchoring case. Assuming that w_e is still large enough so that $\theta_s - \theta_0$ is a small quantity, we can approximate $\sin(\theta_s - \theta_0) \sim \theta_s - \theta_0$. Furthermore, θ_0 is of the order of qA, as in the approximation reported above. It follows that the boundary condition (13) can be approximated, at the first order in qA, as

$$-K\theta_{,z} + w_e(\theta_s - \theta_0) = 0. \tag{20}$$

The function $\theta(x,z)$ solution of Eq. (11), satisfying the boundary conditions (12) and (20), is

$$\theta(x,z) = -\frac{qA}{1+qL}\sin(qx)\exp(-qz), \tag{21}$$

where $L=K/w_e$ is the extrapolation length. Solution (21) reduces to Eq. (17) for $w_e \to \infty$, i.e., for $L \to 0$, as expected.

The equivalent anchoring energy is derived as

$$w = \tfrac{1}{4}Kq\frac{(qA)^2}{1+qL}. \tag{22}$$

Note that the anchoring energy due to the direct interaction of the liquid crystal with the substrate can be considered strong when $qL=qK/w_e \ll 1$, i.e., $w_e \gg qK = 2\pi(K/\lambda)$. The intrinsic anchoring energy of the problem is then $w_i=qK$.

Finally, we wish to mention that a previous analysis[18] has indicated that the theoretical solutions reported above overestimate the equivalent anchoring energy, both in the weak and strong anchoring cases. The errors in estimation are already significant for $qA=1$.

D. Numerical solution

A numerical solution of the problem is always possible, giving the equilibrium conditions by solving a dynamical equation. Nevertheless, care has to be taken into account in the definition of the viscous terms to be added in the bulk Eq. (12) and in the dynamical equation of the boundary condition (3). Also, the convergence of the numerical solution must be considered, before assuming the validity of the dynamical approach to find the equilibrium solution, as will be discussed in the next paragraphs.

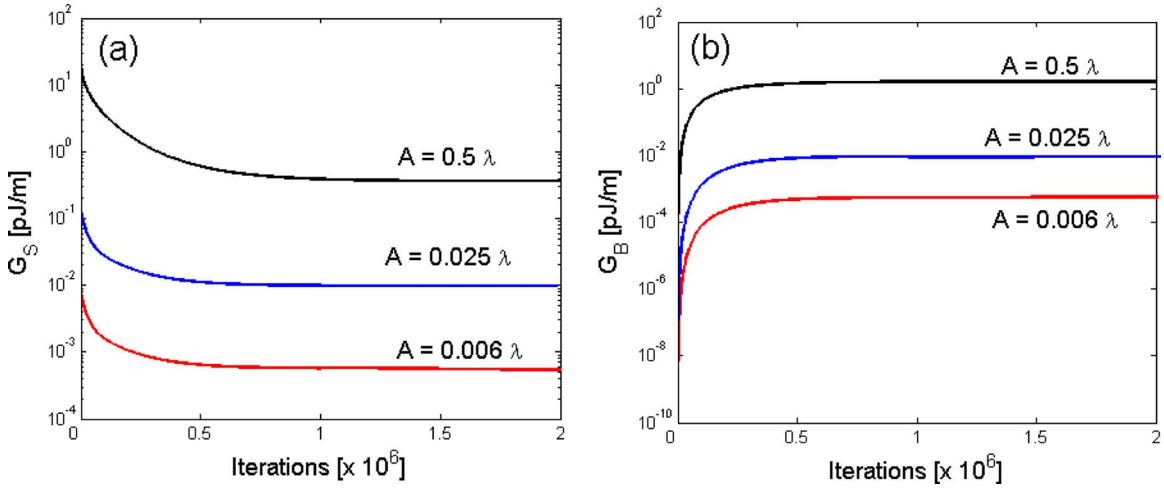

FIG. 2. (Color online) Evolution of the (a) bulk and (b) surface energies as a function of the number of iterations of the numerical scheme. Convergence to an equilibrium value is ensured.

1. Derivation of the dynamical equations

Let us consider an equilibrium state and perturb it by means of external forces. A local deformation $\delta\theta$ is produced, with a resulting work due to the external torque τ_{ext}. Contributions are expected both in the bulk and on the surface,

$$\delta W = \int\int_{\mathcal{R}} \tau_{\text{ext}}^{\text{bulk}} \delta\theta dx dz + \int_{\partial\mathcal{R}} \tau_{\text{ext}}^{\text{surface}} \delta\theta d\ell . \tag{23}$$

If the deformation is quasistatic, the net torque density in the bulk has to be balanced by a torque resulting from the restoring elastic forces, due to the elastic properties of the medium. This internal torque τ_{int} is equal and opposite to τ_{ext}. Therefore

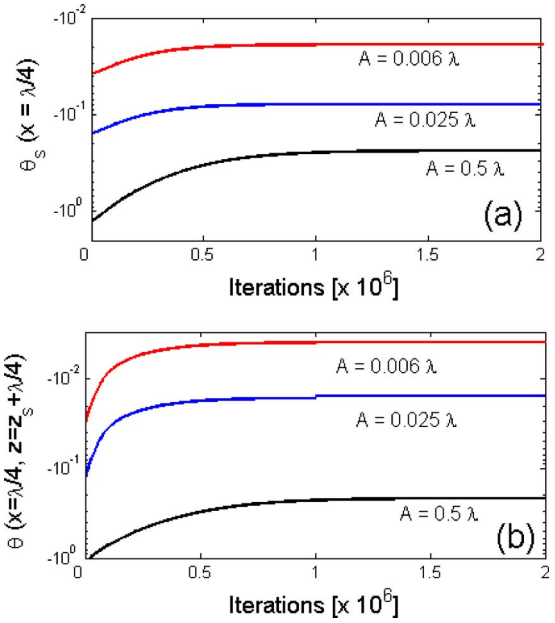

FIG. 3. (Color online) Evolution of the tilt angle in $x=\lambda/4$ (a) on the surface and (b) in the bulk as a function of the number of iterations of the numerical scheme. Convergence to an equilibrium value is ensured.

$$\delta W = -\int\int_{\mathcal{R}} \tau_{\text{int}}^{\text{bulk}} \delta\theta dx dz - \int_{\partial\mathcal{R}} \tau_{\text{int}}^{\text{surface}} \delta\theta d\ell . \tag{24}$$

Finally we observe that $\delta W = \delta F$, given by Eq. (6). Therefore the torque due to elastic forces is

$$\tau_{\text{int}}^{\text{bulk}} = -\frac{\partial f}{\partial \theta} + \nabla \frac{\partial f}{\partial \nabla \theta}$$

$$\tau_{\text{int}}^{\text{surface}} = -\frac{dg}{d\theta_s} - \mathbf{u}\frac{\partial f}{\partial \nabla \theta_s}, \tag{25}$$

in the bulk and on the surface, respectively.

Let us now consider an out of equilibrium system, in presence of dissipation. The latter causes a viscous torque,

$$\tau_{\text{visc}}^{\text{bulk}} = -\eta_B \frac{\partial \theta}{\partial t},$$

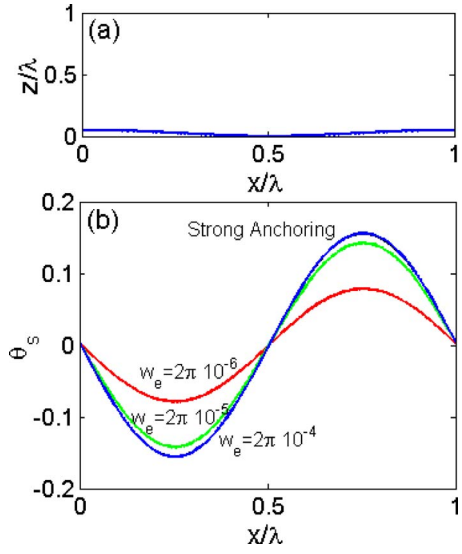

FIG. 4. (Color online) Profile of the (a) surface and (b) distribution at equilibrium of the tilt angles on the surface for different values of the anchoring energy. $A=0.025\lambda$. Note that the strong anchoring and $w_e=2\pi \times 10^{-4}$ J/m^2 profiles are coincident.

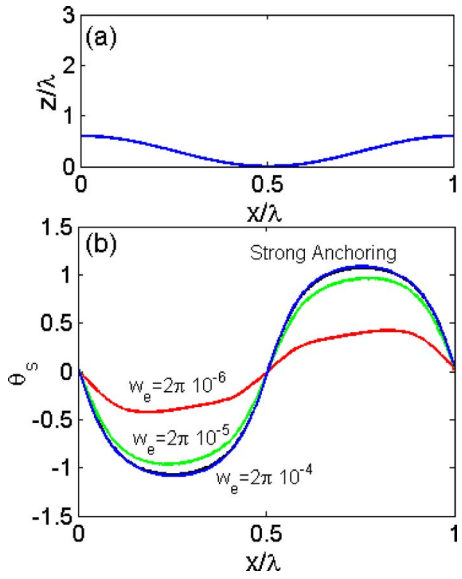

FIG. 5. (Color online) Profile of the (a) surface and (b) distribution at equilibrium of the tilt angles on the surface for different values of the anchoring energy. $A=0.3\lambda$. Note that the strong anchoring and $w_e=2\pi \times 10^{-4}$ J/m^2 profiles are coincident.

$$\tau_{\text{visc}}^{\text{surface}} = -\eta_S \frac{\partial \theta_s}{\partial t}, \tag{26}$$

where we have introduced the bulk and surface viscosities.[25] The dynamical equations are derived by balancing the internal and viscous torques (assuming negligible the inertial properties of the medium),

$$\eta_B \frac{\partial \vartheta}{\partial t} + \frac{\partial f}{\partial \vartheta} - \nabla \frac{\partial f}{\partial \nabla \vartheta} = 0,$$

$$\eta_S \frac{\partial \vartheta_s}{\partial t} + \frac{dg}{d\vartheta_s} + \mathbf{u} \frac{\partial f}{\partial \nabla \vartheta_s} = 0. \tag{27}$$

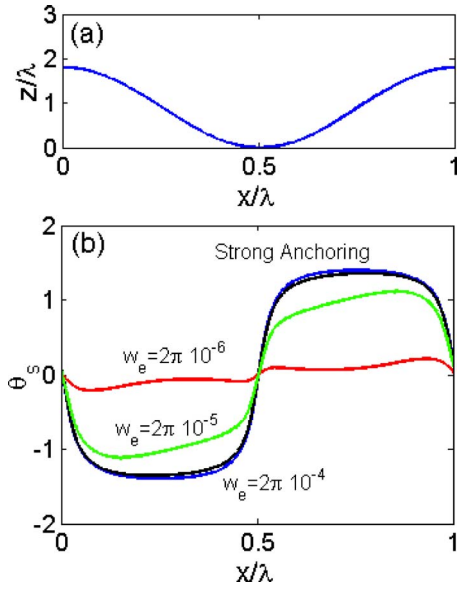

FIG. 6. (Color online) Profile of the (a) surface and (b) distribution at equilibrium of the tilt angles on the surface for different values of the anchoring energy. $A=0.9\lambda$. Note that the strong anchoring and $w_e=2\pi \times 10^{-4}$ J/m^2 profiles are coincident.

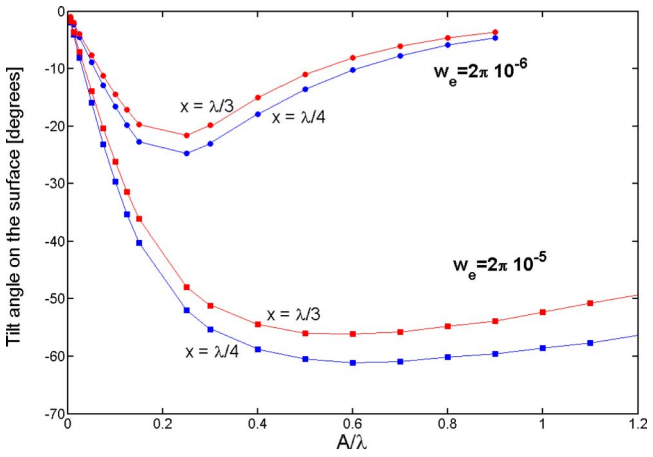

FIG. 7. (Color online) Tilt angle on the surface at equilibrium as a function of the groove amplitude for different anchoring strength and positions. Note the presence of a maximum.

2. Numerical approach

From Eq. (27) and using the definition of f given by Eq. (4), we obtain the equations describing the temporal evolution of the system,

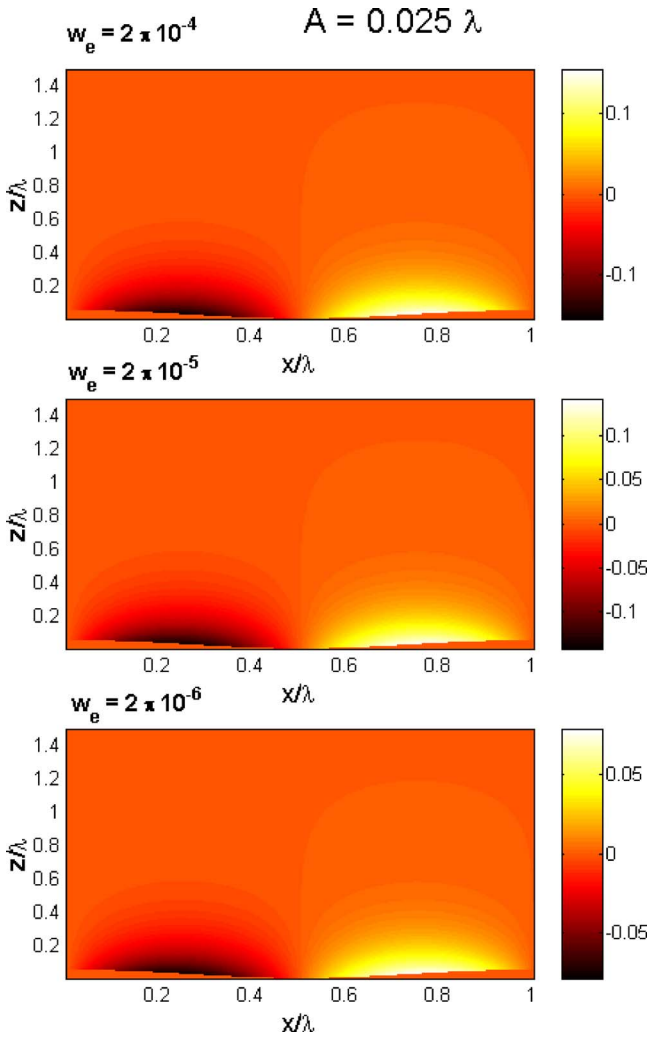

FIG. 8. (Color online) Maps of the tilt angle distribution at equilibrium for different anchoring energies. $A=0.025\lambda$.

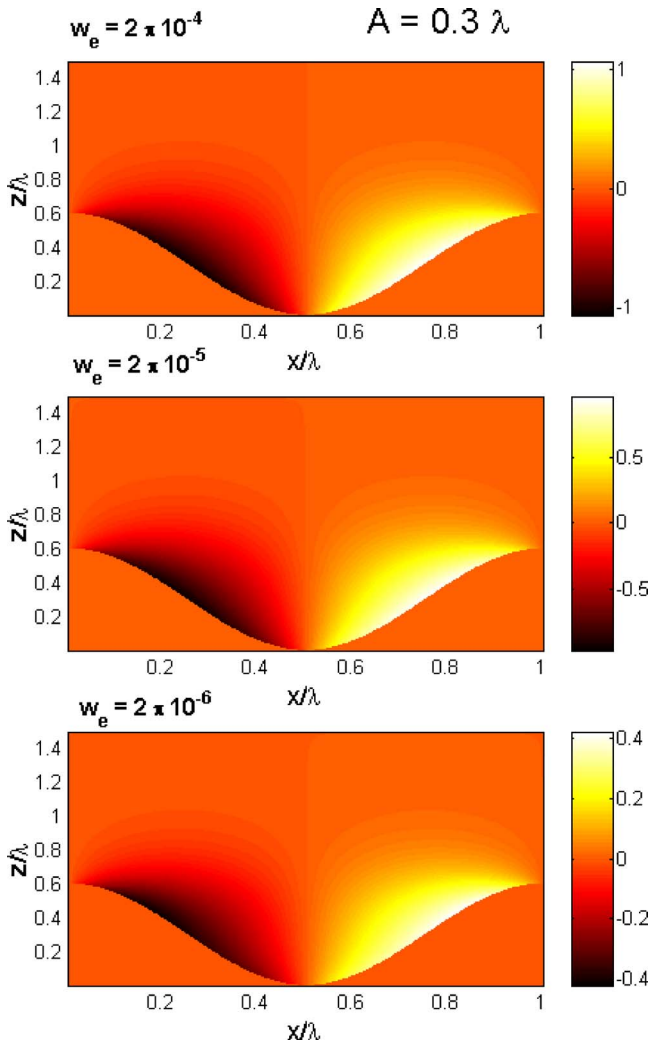

FIG. 9. (Color online) Maps of the tilt angle distribution at equilibrium for different anchoring energies. $A=0.3\lambda$. Note the different scale with respect to Fig. 8.

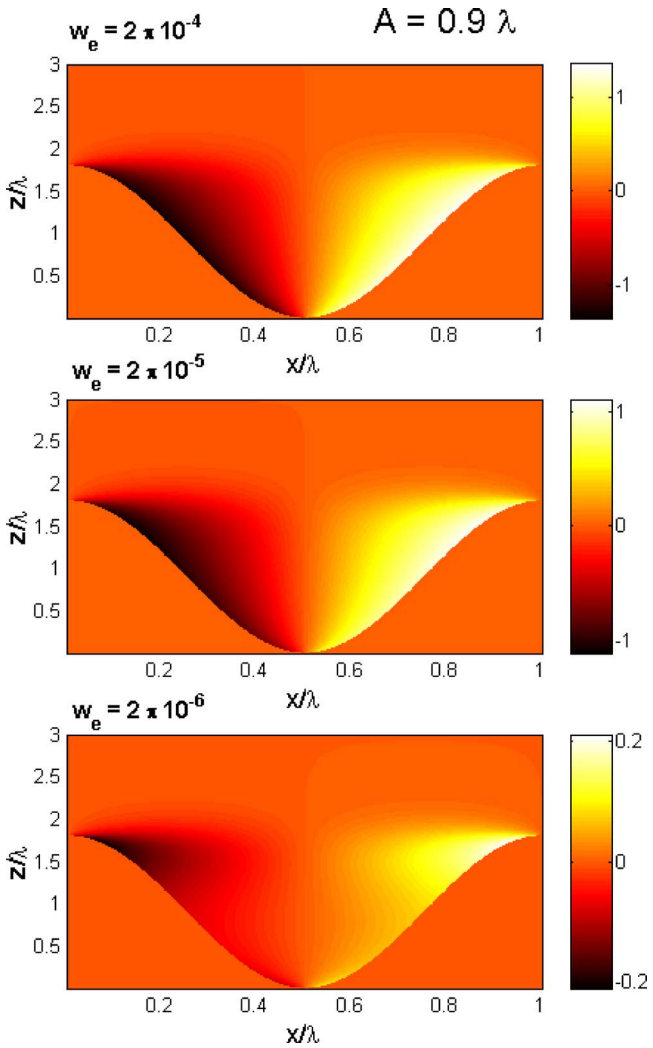

FIG. 10. (Color online) Maps of the tilt angle distribution at equilibrium for different anchoring energies. $A=0.9\lambda$. Note the distortions with respect to Figs. 8 and 9.

$$K(\theta_{,xx}+\theta_{,zz})=\eta_B\frac{\partial\theta}{\partial t}, \tag{28}$$

in the bulk and,

$$K(\sin\theta_0\theta_{,x}-\cos\theta_0\theta_{,z})+\frac{w_e}{2}\sin[2(\theta-\theta_0)]=-\eta_S\frac{\partial\theta}{\partial t}, \tag{29}$$

on the boundaries.

These equations can be solved numerically using a finite difference approach, with a forward scheme for the time derivative and a centered scheme for the space derivative.[26] We have found that a discretization with space step $\lambda/600$ and time step given by $5\times10^{-7}\eta_B/K$ is sufficient to guarantee convergence and stability of the numerical procedure.[27] To this purpose, we have verified the invariance of the results for changes in the discretization adopted and the convergence to the known numerical solutions in the small amplitude limit.

Periodic (along x) boundary conditions are used. For the numerical solution, the boundary condition on the surface opposite to the grooved surface [Eq. (12)] is automatically satisfied, provided the specimen depth (along z) is sufficiently large (three wavelengths). The initial state of the system is arbitrarily defined. We have chosen

$$\theta(x,z;t=0)=\theta_0(x)[3\lambda+z_0(x)-z]/3\lambda,$$

where $\theta_0(x)$ and $z_0(x)$ are given by Eqs. (3) and (1).

To find the actual solution corresponding to the equilibrium state, we let the system evolve until equilibrium, defined by $\partial\theta/\partial t=0$, is reached. Using the equilibrium configuration $\theta(x,z)=\lim_{t\to\infty}\theta(x,z;t)$, we calculate the bulk energy density f by means of Eq. (4), and the total energy F using Eq. (5). Finally, the equivalent anchoring energy strength is evaluated.

We also remark that, as will be clear later, the deformations in the equilibrium configuration are confined to a depth of about one wavelength from the surface. Therefore, a high accuracy is required to numerically calculate space derivatives in this region, which is responsible for the need of a fine discretization of space.

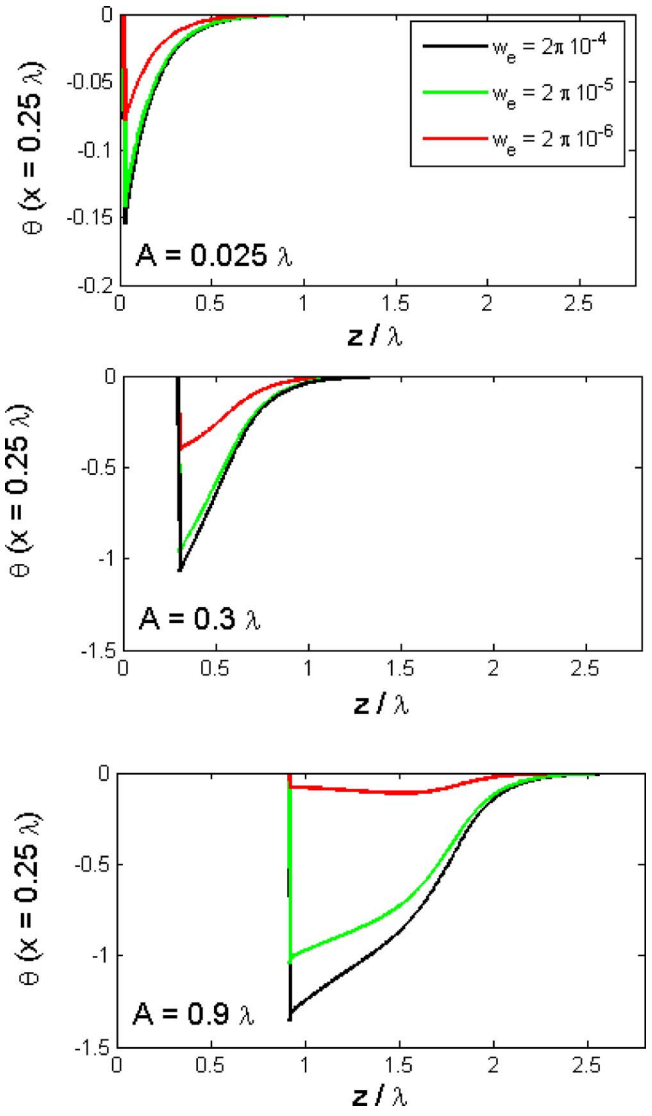

FIG. 11. (Color online) Profiles of the tilt angle distribution in $x=\lambda/4$.

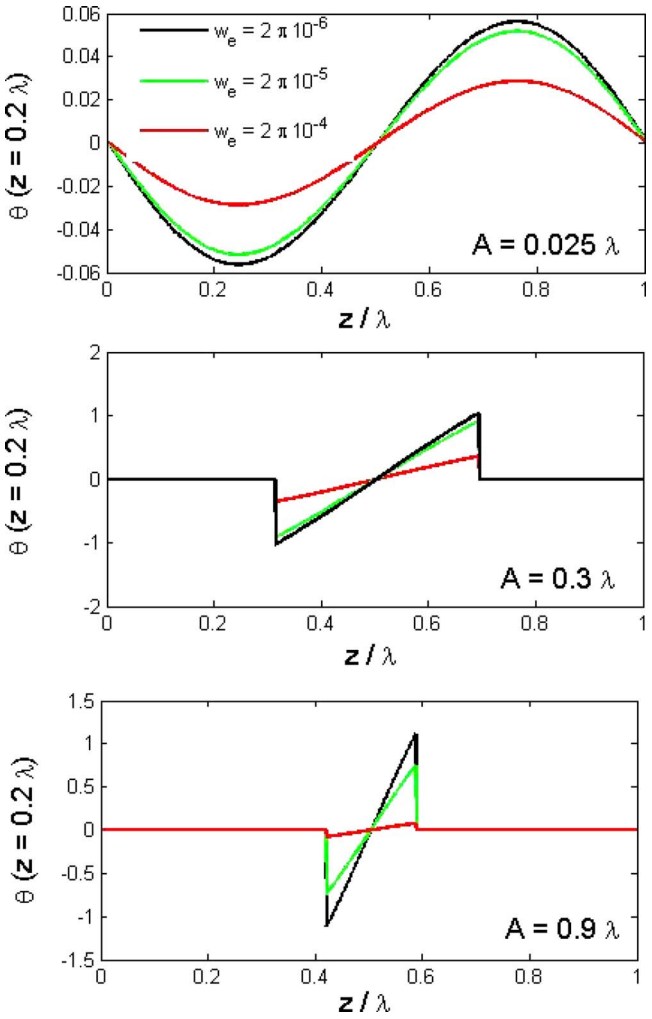

FIG. 12. (Color online) Profiles of the tilt angle distribution in $z=\lambda/5$.

3. Convergence of the solution

We briefly discuss here the convergence of the numerical solution toward an equilibrium state. To this purpose we consider typical values of the parameters: $K=10^{-12}$ J/m, $w_e=2\pi\times10^{-6}$ J/m^2, and $\lambda=1$ μm.[17]

In Fig. 2 the surface (G_S) and bulk (G_B) contributions to the total energy per wavelength are plotted versus the number of iterations of the numerical procedure for different values of the amplitude of the grooves, as reported in the legend [see definitions in Eq. (16)]. Both quantities evolve toward an asymptotic (equilibrium) value, indicating the convergence of the numerical solution. The dynamics of the numerical solution is not a single exponential decay (note the log scale on the y-axes).

To further confirm the validity of the numerical solution, in Fig. 3 the tilt angle on the surface and in the bulk (at a distance $\lambda/4$ from the surface) is reported versus the number of iterations of the numerical solution. Again, convergence to equilibrium is ensured.

III. RESULTS

A. Distribution of the tilt angle

The presence of a weak anchoring at the surface influences the distribution of the tilt angles on the surface and in the bulk of the cell. Such deviations from the behavior predicted by Barbero *et al.*[18] and Berreman[19] are added to those due to the presence of finite amplitude grooves. In this section we have considered typical values for the parameters $K=10^{-12}$ J/m and $\lambda=1$ μm.[17]

In Figs. 4–6 we analyze the equilibrium distribution of tilt angles on the surface for $A=0.025\lambda$, $A=0.3\lambda$, and $A=0.9\lambda$. The solutions in the strong anchoring case [Eq. (3)] and for $w_e=2\pi\times10^{-4}$ J/m^2 are approximately the same for each value of the amplitude of the grooves. Note the deviation from a cosinusoidal profile for large amplitude of the grooves [Figs. 5 and 6] due to the arctan in Eq. (3). In these cases, Berreman's solution is no longer valid. An accurate discussion is reported in Ref. 18. Distortions from the strong anchoring case are evident for both $w_e=2\pi\times10^{-5}$ J/m^2 and $w_e=2\pi\times10^{-6}$ J/m^2. For intermediate amplitudes of the grooves (Fig. 5), θ_s assumes a nonsymmetric profile. The distribution becomes more complex when the anchoring is very weak and the groove amplitude is large. Here, maxima appear close to the positions where the tilt angle is zero (x

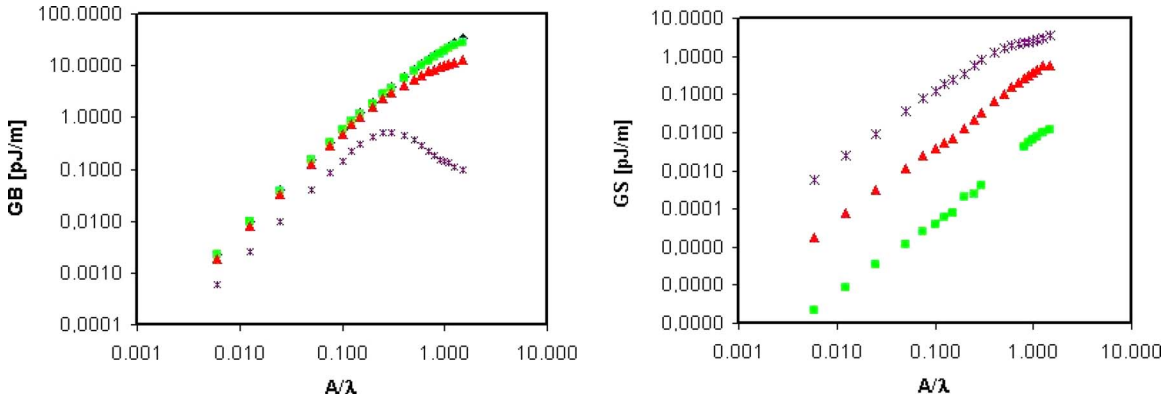

FIG. 13. (Color online) Bulk and surface energy contributions as a function of the groove amplitude for different anchoring strengths. Note the maximum in the bulk energy and the evolution toward an asymptotic value of the surface energy for the weaker anchoring strength.

$=0,\lambda/2,\lambda$). In each case the tilt angles on the surface are smaller when the anchoring is weaker, as expected.

It is interesting to observe that the maximum tilt angle on the surface is in $x=\lambda/4$, when the anchoring is strong. Weakening the anchoring energy causes a deformation in the distribution of the tilt angles on the surface, with resulting shift in the position of the maximum toward $x=0$ and the emergence of a maximum close to $x=\lambda/2$. At the same time, for fixed anchoring strength, the shift in the maximum position increases with the increasing amplitude of the grooves. On the contrary, the surface tilt angle in $x=0$ and $x=\lambda/2$, due to symmetry reasons, remains always zero independently from both the groove amplitude and the anchoring energy.

As a result of the observation reported above, we expect two competing mechanisms to take place on the surface. An increase in the amplitude of the groove forces an increase in the surface tilt angle, at the same time the effects due to the weak anchoring produce a shift in the maximum (increasing with amplitude), hence forcing a reduction in the tilt angle on the surface. We can expect that, as $A\rightarrow\infty$, the position of the maximum goes to $x=0$, hence $\theta_s^{\max}$ goes to 0. This result is confirmed by Fig. 7, where we report the tilt angle on the surface in $x=\lambda/4$ and $x=\lambda/3$ as a function of the groove amplitude for $w_e=2\pi\times10^{-5}$ J/m^2 (squares) and $w_e=2\pi\times10^{-6}$ J/m^2 (circles).

The distributions of the tilt angles at equilibrium in the bulk are reported in Figs. 8–10, for $A=0.025\lambda$, $A=0.3\lambda$, and $A=0.9\lambda$. For small and intermediate values of the amplitude of the grooves (Figs. 8 and 9), the effect of weakening the anchoring strength is limited to a reduction in the tilt angles, without remarkable changes on the profile. For $A=0.9\lambda$, on the contrary, the spatial distribution is also affected, see bottom plot of Fig. 9. In this case it is to be noted that the tilt angles are very small compared to the other cases, as will also be discussed in the Sec. III B.

In Figs. 11 and 12, we report the profile of the tilt angle in the bulk along a vertical line ($x=\lambda/4$) and a horizontal line ($z=\lambda/8$), respectively. The expected exponential decay along z and cosine profile along x are found for small amplitudes of the grooves (see upper plots of Figs. 10 and 11). Significant deviations are present for large amplitudes of the grooves (middle and bottom plots), even though in all cases the tilt angle decays to zero in approximately one wavelength. Again the case $A=0.9\lambda$ and $w_e=2\pi\times10^{-6}$ J/m^2 presents an anomalous behavior: The profile along the z-direction is no longer monotonously decreasing.

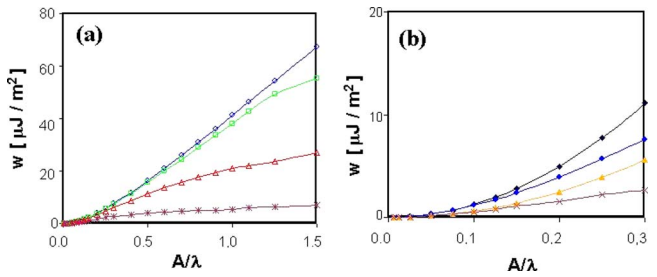

FIG. 14. (Color online) (a) Equivalent anchoring energy as a function of the groove amplitude. (b) Small amplitude limit for the strong anchoring case and weaker anchoring strength. The comparison with theoretical expectations is very good.

B. Evaluation of the equivalent anchoring energy

The bulk and surface contributions (G_B and G_S, respectively) to the total energy in one period are analyzed in Fig. 13. Given the equilibrium distribution of the tilt angles, the energies are derived according to Eq. (16). The bulk elastic energy (per wavelength) diminishes with the decreasing anchoring energy w_e, for any amplitude of the grooves. In the case $w_e=2\pi\times10^{-6}$ J/m^2 (violet stars), G_B increases with increasing A, up to maximum and then starts decreasing again [Fig. 12(a)]. The presence of a maximum seems to be also present for the other values of w_e, albeit the amplitudes analyzed here are too small to reach it. As expected, G_B in the case $w_e=2\pi\times10^{-4}$ J/m^2 (blue circles) is the same as that for the strong anchoring case (black circles). The surface energy G_S increases for increasing A for all the cases considered. When the anchoring is weak, as expected, both G_S and G_B are smaller.

Finally, in Fig. 14 we calculate the equivalent anchoring energy

$$w=2\frac{G_B+G_S}{\lambda}.$$

w increases with the increasing amplitude of the grooves, being always much smaller than that in the strong anchoring

case. Also, see Fig. 13(b), the calculated equivalent anchoring energy is the same as that theoretically expected [Eq. (22)] in the small amplitude limit.

IV. CONCLUSION

We have analyzed the effect of the anchoring at the surface on the tilt angle field in a liquid crystal cell in contact with a corrugated surface. The equilibrium distribution in the sample has been derived using a numerical solution and the equivalent anchoring energy of the system has been calculated. Our results indicate a nontrivial effect on the distribution of the tilt angles on the surface when diminishing the strength of the anchoring energy. In particular, the position of the maxima deformation does no longer correspond to those of the maximum slope in the profile and more maxima appear in the profile of the tilt angle on the surface.

As a result of our observation, the equivalent anchoring energy does not diverge with the increasing amplitude of the grooves, as it could have been trivially expected. Rather, an asymptotic value is expected, with a monotonous increase with amplitude. The plateau is already reached for low values of the groove amplitude if the anchoring is very weak. More intriguing is the fact that the bulk energy density in the sample presents a maximum as a function of the surface amplitude and then diminishes, going to zero for infinite amplitude of the grooves.

Our result indicates that care has to be taken when using the Berreman approximation in the interpretation of experimental data. Indeed, even at low values of amplitude, the Berreman estimation can be largely incorrect when the treatment of the surface is such to diminish the anchoring energy strength.

Of course additional features, not considered here, are important for a correct estimation of the behavior. Among them the anisotropy of the elastic constants, which is expected only to modify quantitatively the results presented here, and the effects due to azimuthal distortions. Further studies are in progress in the latter direction.

[1] J. Cognard, Mol. Cryst. Liq. Cryst. Suppl. Ser. **A5**, 1 (1982).
[2] J. Stöhr, M. G. Samant, J. Lüning, A. C. Callegari, P. Chaudhari, J. P. Doyle, J. A. Lacey, S. A. Lien, S. Purushothaman, and J. L. Speidell, Science **292**, 2299 (2001).
[3] G. P. Bryan-Brown, C. V. Brown, I. C. Sage, and V. C. Hui, Nature (London) **392**, 365 (1998).
[4] C. J. Newsome, M. O'neill, R. J. Farley, and G. P. Bryan-Brown, Appl. Phys. Lett. **72**, 2078 (1998).
[5] X. Lu, F. K. Lee, P. Sheng, H. S. Kwok, V. Chigrinov, and O. K. C. Tsui, Appl. Phys. Lett. **88**, 243508 (2006).
[6] F. S. Y. Yeung, F.-C. Xie, J. T.-K.Wan, F. K. Lee, O. K. C. Tsui, P. Sheng, and H.-S. Kwok, J. Appl. Phys. **99**, 124506 (2006).
[7] L. Komitov, G. P. Bryan-Brown, E. L. Wood, and A. B. J. Smout, J. Appl. Phys. **86**, 3508 (1999).
[8] G. P. Bryan-Brown, E. L. Wood, and I. C. Sage, Nature (London) **399**, 338 (1999).
[9] J. van Haaren, Nature (London) **392**, 331 (1998).
[10] See e.g., Th. Rasing and I. Musevic, *Surfaces and Interfaces in Liquid Crystals* (Springer, Berlin, 2004), and references contained therein.
[11] W. M. Gibbons, P. J. Shannon, S. T. Sun, and B. J. Swetlin, Nature (London) **351**, 49 (1991).
[12] M. Schadt, H. Seiberle, and A. Schuster, Nature (London) **381**, 212 (1996).
[13] M. Talarico, G. Carbone, R. Barberi, and R. Bartolino, Appl. Phys. Lett. **85**, 528 (2004).
[14] B. T. Hallam and J. R. Sambles, Liq. Cryst. **27**, 1207 (2000).
[15] P. Pagliusi, C. Y. Shen, and Y. R. Shen, J. Chem. Phys. **125**, 201104 (2006).
[16] D.-H. Chung, H. Takezoe, B. Park, Y. Jung, H.-k. Hwang, S. Lee, K.-J. Han, S.-H. Jang, and H. Yokoyama, Jpn. J. Appl. Phys., Part 1 **39**, 1252 (2000).
[17] D.-H. Chung, T. Fukuda, Y. Takanishi, K. Ishikawa, H. Matsuda, H. Takezoe, and M. A. Osipov, J. Appl. Phys. **92**, 1841 (2002).
[18] G. Barbero, A. S. Gliozzi, M. Scalerandi, and L. R. Evangelista, Phys. Rev. E **77**, 051703 (2008).
[19] D. W. Berreman, Phys. Rev. Lett. **28**, 1683 (1972).
[20] P. G. de Gennes and J. Prost, *The Physics of Liquid Crystals* (Oxford Sciences, Oxford/Clarendon, Oxford, 1993).
[21] S. Faetti, Phys. Rev. A **36**, 408 (1987).
[22] J. B. Fournier and P. Galatola, Phys. Rev. E **60**, 2404 (1999).
[23] J. Fukuda, M. Yoneya, and H. Yokoyama, Phys. Rev. Lett. **98**, 187803 (2007).
[24] G. Barbero and L. Evangelista, *An Elementary Course on the Continuum Theory for Nematic Liquid Crystals* (World Scientific, Singapore, 2001).
[25] A. M. Sonnet, E. G. Virga, and G. E. Durand, Phys. Rev. E **62**, 3694 (2000).
[26] G. Kaniadakis, P. P. Delsanto, and C. A. Condat, Math. Comput. Modell. **17**, 31 (1993).
[27] F. C. M. Freire, G. Barbero, and M. Scalerandi, Phys. Rev. E **73**, 051202 (2006).